Scilight

Smart Materials and Devices

https://www.sciltp.com/journals/smd

Article

Corrosion Performance of $Al_{0.1}CoCrFeNi$ High Entropy Alloy in Liquid Lead-Bismuth Eutectic at Different Temperatures

Songqin Xia [1,*], Yimin Yang [2], Baoying Wang [1] and Xuan Zuo [1]

[1] School of Nuclear Science and Engineering, North China Electric Power University, Beijing 102206, China
[2] School of Mechanical Engineering, Qinghai University, Xining 810016, China
* Correspondence: sqxia@ncepu.edu.cn

How To Cite: Xia S, Yang Y, Wang B, Zuo X. Corrosion Performance of $Al_{0.1}CoCrFeNi$ High Entropy Alloy in Liquid Lead-Bismuth Eutectic at Different Temperatures. *Smart Materials Devices* **2026**, *1*(1), 4.

Received: 1 December 2025
Revised: 9 January 2026
Accepted: 12 January 2026
Published: 22 January 2026

Abstract: To investigate the applicability of the $Al_{0.1}CoCrFeNi$ high entropy alloy (HEA) in liquid lead-bismuth eutectic (LBE) environments, this study systematically examined the tensile mechanical properties and corrosion behavior of the alloy at temperatures of 350 °C, 450 °C, and 550 °C. The results showed a significant temperature dependence of the alloy's mechanical properties and fracture mode: At 350 °C and 450 °C, a protective oxide film dominated by Al_2O_3 and Cr_2O_3 forms on the alloy surface, endowing the alloy with high tensile strength (up to 1090 MPa at 350 °C) and excellent ductility (with fracture strain of 10% at 350 °C), ultimately resulting in ductile fracture. At 550 °C, the oxide film undergoes slight damage, accompanied by mild dissolution corrosion. Accordingly, Al and Cr elements dissolve, which in turn triggers liquid metal embrittlement (LME), resulting in a reduction of the alloy's tensile strength to 410 MPa, a decrease in fracture strain to 5%, and the onset of brittle fracture. In addition, no obvious element segregation or massive element loss was observed in the alloy matrix at all test temperatures, indicating that the alloy possesses good chemical stability. This study provides an important reference for the application of the $Al_{0.1}CoCrFeNi$ HEA in LBE environments.

Keywords: high entropy alloy; liquid metal embrittlement; corrosion; oxidation

1. Introduction

LBE ($Pb_{44.5}Bi_{55.5}$, wt.%, mass fraction) is an efficient heat transfer fluid. Due to its excellent inherent safety and sustainability, it is regarded as a candidate coolant for the fourth-generation lead-cooled fast reactor (LFR) [1–3]. However, the widespread application of LBE-cooled fast reactors is hindered by the incompatibility issues between steel and LBE. This problem is mainly reflected in two aspects: liquid metal corrosion (LMC) and LME [4,5].

LMC occurs in various ways, depending on factors such as temperature, the concentration of dissolved oxygen in liquid LBE, and the chemical composition of the steel [6–10]. Ferritic/martensitic (F/M) steel is considered a promising structural material for components such as fuel claddings in LBE cooled reactors due to its good strength, toughness, and irradiation resistance [11]. However, at around 350 °C, LME occurs in F/M steels (such as T91 and HT9) in the LBE environment, which accelerates the initiation and propagation of cracks [12–16]. Accordingly, the ductility and toughness of the material will decrease sharply. LMC occurs not only in F/M steels but also in austenitic stainless steels (such as 316 L and 15-15 Ti). Specifically, when the LBE is in an oxygen-rich state, the corrosion is manifested as oxidation on the material surface. When the LBE is oxygen-poor, the corrosion is manifested as the selective leaching of elements such as nickel, manganese, chromium, and iron in the steel [17]. Irradiation will further exacerbate the adverse effects brought about by LMC and LME [18,19]. These problems can endanger the safe operation of the reactor. LBE-cooled fast reactors have many remarkable

advantages. To fully utilize these advantages, there is an urgent need to explore new materials that can exhibit stronger tolerance in the harsh high-temperature LBE environment. High entropy alloys (HEAs), with their unique microstructures and excellent properties, are highly promising to be the key to solving this problem. In sharp contrast to traditional alloys, which usually contain only a few major elements, HEAs are multi-component alloys that contain at least five major metallic elements, and the molar ratios of these elements are nearly equal [20]. A large number of studies have shown that HEAs possess excellent mechanical properties [21–23], high corrosion resistance and stress corrosion cracking resistance [24–26], as well as good irradiation resistance [27,28].

The $Al_xCoCrFeNi$ alloy is one of the most extensively studied HEA systems due to its microstructure and mechanical properties can be flexibly tailored by adjusting the aluminum (Al) content [29,30], and the alloy can form a passive aluminum oxide film, which has been proven to be an effective corrosion barrier [31]. Existing research on $Al_xCoCrFeNi$ series HEAs in LBE environments has mainly focused on medium-to-high Al content (x = 0.3–0.4) systems [32], these alloys form a dual FCC + BCC phase structure, exhibiting relatively high strength but compromised ductility. In contrast, the low Al content (x = 0.1) adopted in this study ensures the alloy maintains a single FCC phase. For liquid LBE environments, this low Al content avoids the brittleness issue of thick oxide films in high-Al HEAs and reduces the risk of oxide film spallation under tensile stress, thereby filling the research gap in the application of low-Al HEAs in LBE-cooled reactors. The high ductility and LME resistance of the low-Al alloy provide a novel compositional design strategy for developing nuclear structural materials with both mechanical reliability and environmental compatibility.

2. Materials and Experimental Details

2.1. Material Preparation

In this study, aluminum (Al), cobalt (Co), chromium (Cr), iron (Fe), and nickel (Ni), with a purity of ≥ 99.9 weight percent (wt.%) were used as raw materials. The specific preparation process is as follows:

First, the $Al_{0.1}CoCrFeNi$ samples were fabricated using vacuum levitation melting (VLM).

Second, longitudinal cold rolling (CR) was performed with a 70% thickness reduction. Then, the cold-rolled samples were annealed at 600 °C for 2 h, followed by direct water quenching from 600 °C to room temperature. It should be noted that all samples were placed in a vacuum-sealed environment before being placed inside a muffle furnace.

Finally, in accordance with the dimensional requirements shown in Figure 1a, wire electrical discharge machining was used to process the samples into dog-bone-shaped tensile specimens with dimensions of 0.75 mm × 5 mm × 1.5 mm (thickness × gauge length × width), and the LBE tensile tests were conducted, and the tensile testing machine used is shown in Figure 1 b.

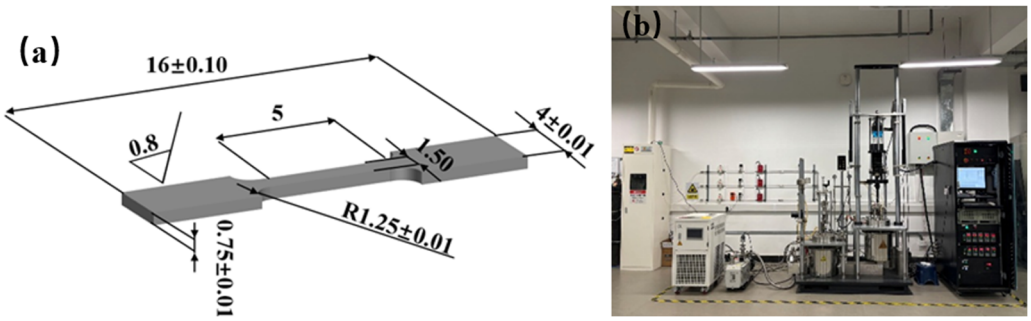

Figure 1. (**a**) Dimensions of the tensile specimen; (**b**) Tensile test instrument.

2.2. LBE Tensile Experiment

The tensile tests of $Al_{0.1}CoCrFeNi$ were carried out in a saturated LBE and an argon environment at a constant strain rate of 2×10^{-6} s^{-1}. This experiment primarily focused on the influence of tensile stress on the corrosion behavior of $Al_{0.1}CoCrFeNi$ in a LBE at 350 °C, 450 °C, and 550 °C. The data acquisition system recorded the force and displacement at specific intervals. All tensile tests continued until the samples fractured. Prior to the test, the samples were respectively heated to 350 °C, 450 °Cand 550 °C, then held at temperature and immersed in static LBE for 24 h. The specific details of the tensile tests are shown in Figure 2.

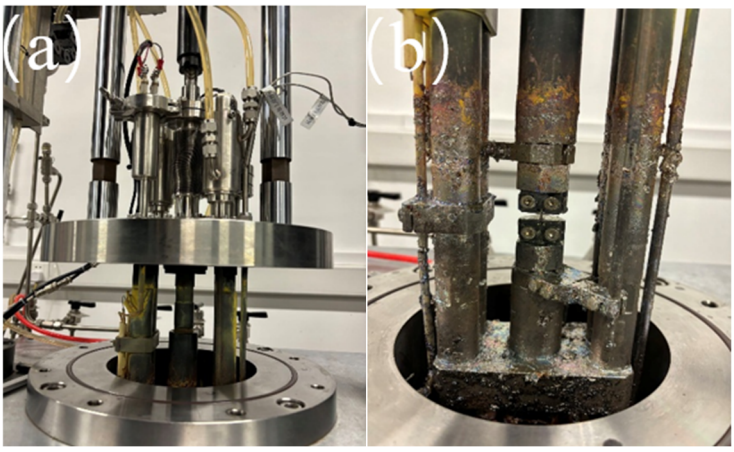

Figure 2. Details of the experimental instrument. (**a**) From bottom to top, the lower circular cavity is the core reaction chamber, designed to hold samples and corrosive media. (**b**) The sample is fixed by a metal fixture, which also displays a corrosion layer on its surface.

2.3. Microstructure Characterization

After the tensile test is completed in the liquid LBE, the liquid LBE alloy remains on the surface of the specimen, and the cross-section of the specimen is polished. Then, a scanning electron microscope (Thermo Fisher Scientific Inc., 168 Third Avenue, Waltham, MA, USA, Model: Helios 5 CX) is used to observe and analyze the surface corrosion and fracture morphology. EDS is employed to analyze the LBE corrosion of the fractured specimen.

3. Results

3.1. Engineering Stress-Strain Curves

Figure 3 shows the engineering tensile stress-strain curves of the $Al_{0.1}$CoCrFeNi HEA in liquid LBE at 350 °C, 450 °C, and 550 °C. It can be observed that the alloy exhibits good yield strength and excellent ductility at the test temperatures of 350 °C and 450 °C. At all three test temperatures, serrated fluctuations appear in all curves, with the phenomenon being more pronounced at 350 °C. At 350 °C, the tensile strength of the alloy is 1090 MPa, and the fracture strain is 10%. This indicates that the $Al_{0.1}$CoCrFeNi HEA is less deteriorated by LME caused by LBE at 350 °C, proving that the surface oxide film can delay the effect of LBE to a certain extent. As the test temperature gradually increases to 550 °C, the tensile strength and strain at fracture of the alloy drop sharply to 410 MPa and 5%, respectively, which indicates that typical LME damage has occurred.

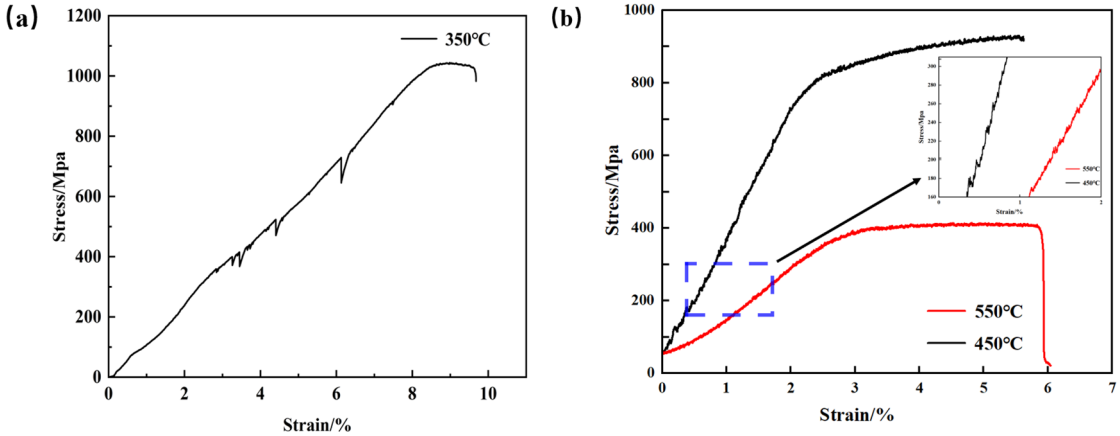

Figure 3. (**a**) Engineering stress-strain curve at 350 °C; (**b**) Engineering stress-strain curves at 450 °C and 550 °C.

3.2. Fracture Analysis and Corrosion Morphology

The fracture images of the $Al_{0.1}$CoCrFeNi alloy tested in liquid LBE at 350 °C and 450 °C are shown in Figure 4a–d. A large number of uniformly distributed dimples can be seen, which are distributed in a fibrous or network pattern, characteristic of ductile fracture, indicating the $Al_{0.1}$CoCrFeNi alloy exhibits good plasticity at 350 °C and 450 °C, with obvious plastic deformation occurring before fracture, and is less susceptible to LME.

This is consistent with the fact that the face-centered cubic (FCC) austenite phase in steel is less susceptible to LME in the presence of liquid LBE [19,33]. However, when the temperature rises to 550 ℃, it is found that the alloy undergoes obvious brittle fracture, as shown in Figure 4e,f. The fracture surface is relatively flat, with no obvious dimples, showing brittle characteristics of cleavage or intergranular fracture. This indicates that the alloy undergoes sudden brittle fracture in the liquid LBE environment at 550 ℃, with a significant decrease in plasticity, suggesting that the $Al_{0.1}$CoCrFeNi alloy is eroded by LBE at 550 ℃. It can be seen from Figure 4a,b that the fracture surfaces of the $Al_{0.1}$CoCrFeNi alloy after tensile testing in LBE are mainly covered with micro-pits, with no obvious signs of LME. This indicates that under the current test conditions, the $Al_{0.1}$CoCrFeNi alloy is not easily affected by the typical LME effect at 350 ℃.

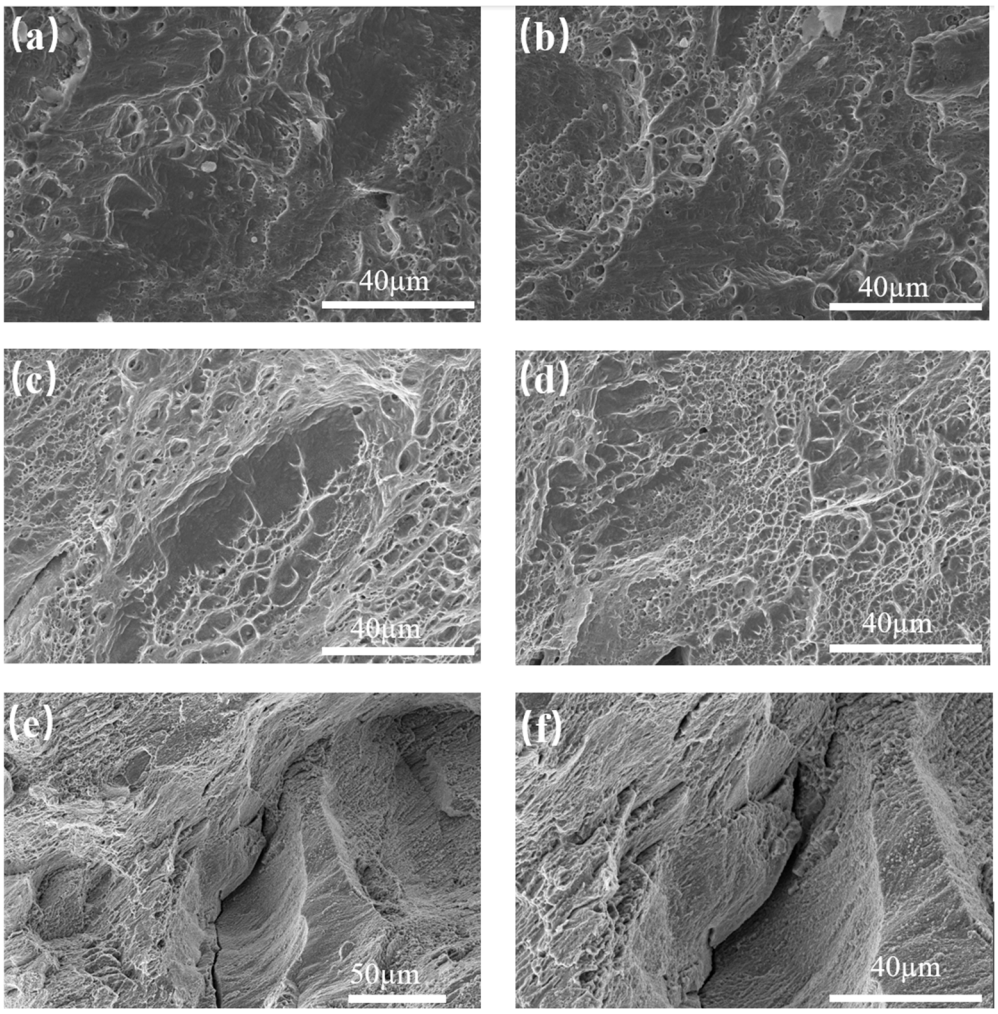

Figure 4. SEM fracture morphologies of specimens after tensile testing under LBE at different temperatures, (**a**,**b**) correspond to 350 ℃, (**c**,**d**) correspond to 450 ℃, and (**e**,**f**) correspond to 550 ℃.

4. Discussion

4.1. Temperature-Dependent Transition of Oxide Stability, Dissolution Behavior, and LME Susceptibility

At 350 ℃, as shown in Figure 5 by Scanning Electron Microscope (SEM) and Energy Dispersive X-ray Spectroscopy (EDS), we can observe that the O element is significantly enriched near the interface. We speculate that an oxide layer dominated by Al and Cr oxides (such as Al_2O_3 and Cr_2O_3) is formed on the alloy surface, which is a direct indication of oxidative corrosion of the alloy. This oxide layer can effectively prevent the penetration of liquid LBE (Pb, Bi) into the alloy matrix (the signals of Pb and Bi elements are extremely weak), demonstrating a certain degree of interfacial stability and corrosion resistance, and effectively preventing LME.

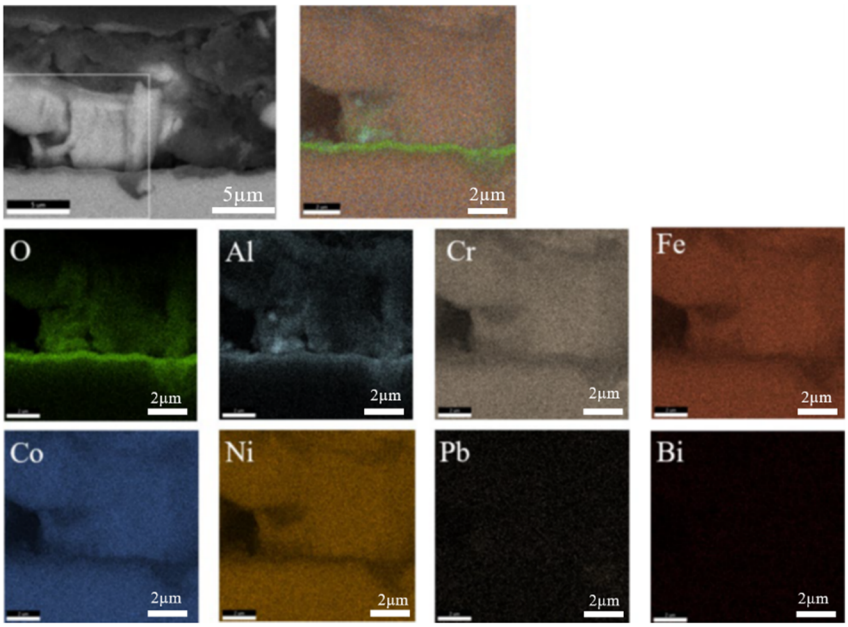

Figure 5. Cross-sectional SEM image and EDS elemental mappings of the specimen after exposure to LBE at 350 °C.

The test results at 450 °Cand 550 °Care shown in Figures 6 and 7. It can be observed that at 450 °C, similar to that at 350 °C, the oxide layer effectively prevents the penetration of LBE (Pb, Bi) into the alloy matrix. However, as the temperature rises to 550 °C, the oxide layer is no longer intact, and element dissolution occurs, resulting in dissolution corrosion. As illustrated in Figure 8, significant enrichment of Pb and Bi is observed at the grain boundaries, whereas no such penetration phenomenon is detected at 350 °C and 450 °C. Due to the enhancement of dissolution corrosion, liquid metal embrittlement (LME) occurs, leading to brittle fracture, as shown in Figure 4e,f.

It has been reported that significant dissolution corrosion usually occurs in austenitic stainless steels at temperatures above 450 °C and in F/M steels at temperatures above 550 °C [33]. In general, however, alloying elements such as Al, Cr, Fe, Co, and Ni (matrix elements of the HEA) are distributed in correspondence with the alloy matrix region, with no obvious element segregation or massive dissolution and loss observed. This indicates that the alloy matrix exhibits good chemical stability in liquid LBE environments at different temperatures and does not undergo severe compositional degradation due to the effect of LBE.

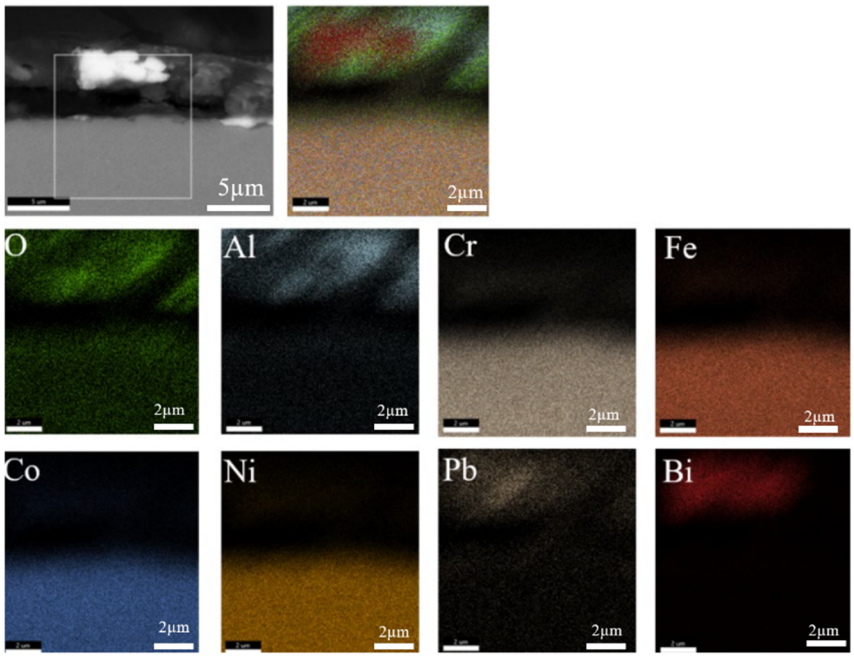

Figure 6. Cross-sectional SEM image and EDS elemental mappings of the specimen after exposure to LBE at 450 °C.

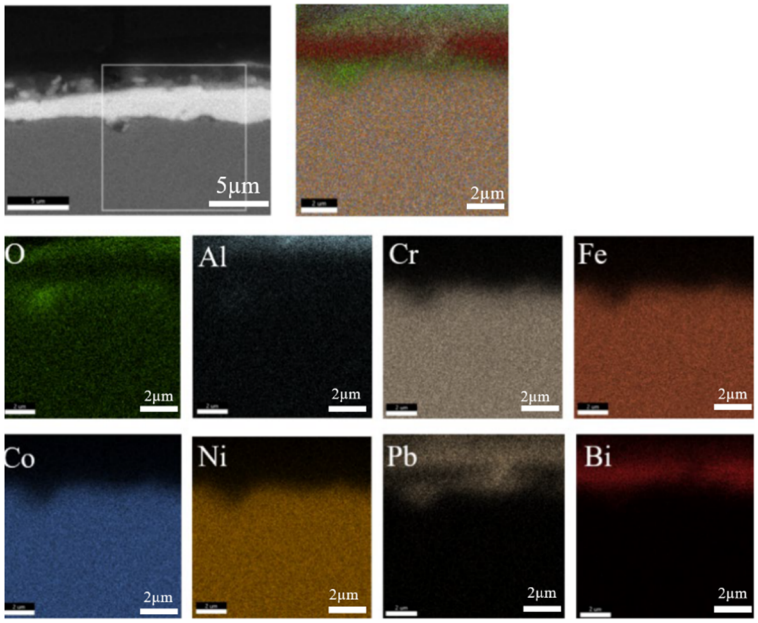

Figure 7. Cross-sectional SEM image and EDS elemental mappings of the specimen after exposure to LBE at 550 °C.

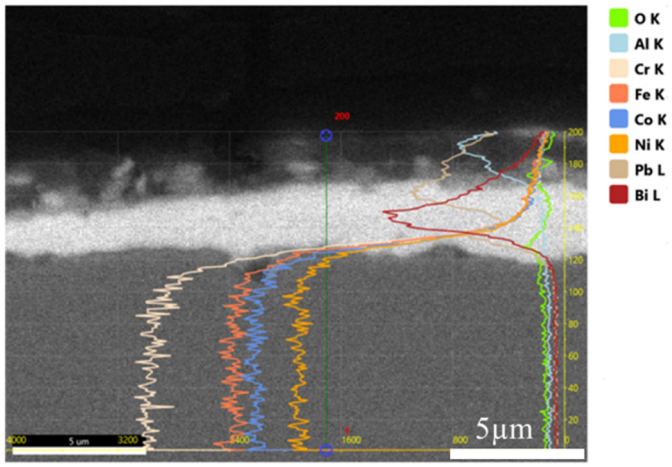

Figure 8. Cross-sectional SEM-EDS line scan after LBE exposure at 550 °C.

4.2. Corrosion Mechanism and Stability Analysis

The corrosion of HEAs in LBE is a complex multi-stage process involving key steps such as dissolution, oxidation, and grain boundary diffusion. These steps interact and synergize with each other, collectively determining the corrosion degree and corrosion rate of structural materials.

In the LBE environment, the corrosion behavior of the $Al_{0.1}CoCrFeNi$ alloy exhibits a distinct temperature-driven mechanism, it should be noted that the identification of the surface oxide layer in the present work is primarily based on SEM/EDS observations, which provide information on elemental distribution rather than definitive phase identification. Nevertheless, under oxygen-controlled LBE environments (typically 10^{-7}–10^{-6} wt.% O), both thermodynamic analyses and extensive experimental evidence consistently indicate that Al and Cr exhibit the strongest affinity for oxygen among the constituent elements, leading to the preferential formation of Al_2O_3 and Cr_2O_3 as the most stable oxide phases [15–17]. Previous studies on Fe-Cr, FeCrAl alloys, and $Al_xCoCrFeNi$ HEAs exposed to LBE have demonstrated that these Al/Cr-rich oxide layers are dense, adherent, and highly effective in suppressing Pb/Bi penetration and mitigating LME [34,35].

In the temperature range of 350–450 °C, the formation of a protective oxide film is the dominant corrosion mechanism in the LBE environment. In oxygen-containing LBE, Al and Cr preferentially oxidize to form a dense oxide layer with low solubility and a stable interface, which effectively blocks the penetration of Pb and Bi. SEM/EDS results show pronounced oxygen enrichment at the interface accompanied by negligible Pb/Bi signals, indicating that the oxide layer suppresses liquid metal ingress and mitigates LME, thereby allowing the alloy to retain good plasticity and ductility. Owing to the relatively low Al content in the present alloy

($Al_{0.1}$CoCrFeNi with a single FCC phase), the excessive oxide thickness and spallation commonly observed in high-Al HEAs are avoided, leading to reduced interfacial stress and improved chemical stability.

When the temperature increases to 550 ℃, dissolution corrosion and diffusion processes gradually become dominant. The oxide layer undergoes local destabilization, accompanied by the selective dissolution of Al and Cr, which enhances the chemical reactivity between the alloy matrix and LBE. Pb and Bi subsequently diffuse and accumulate along grain boundaries, which serve as preferential sites for the initiation of LME, ultimately resulting in brittle fracture and interfacial failure. Consequently, the corrosion mechanism transitions from oxidation-controlled behavior at lower temperatures to dissolution corrosion and interfacial diffusion control at elevated temperatures, consistent with the temperature-dependent variations in interfacial elemental distributions and mechanical responses observed in this study.

When the temperature further rises to a high-temperature range, not only do the rates of dissolution corrosion and oxidation reactions continue to increase, but also the internal structure of the material changes, such as grain growth and grain-boundary migration. This leads to a change in the energy state at the grain boundaries, which is more conducive to the diffusion of LBE atoms along the grain boundaries, exacerbating intergranular corrosion and making the embrittlement of the material more serious, eventually leading to fracture [36].

5. Conclusions

The corrosion behavior of $Al_{0.1}$CoCrFeNi HEA in LBE was investigated at temperatures of 350 ℃, 450 ℃, and 500 ℃, and the following conclusions were drawn:

(1). In LBE, the mechanical properties and fracture behavior of the alloy are strongly temperature-dependent. At 350 ℃ and 450 ℃, it retains high tensile strength (up to 1090 MPa at 350 ℃) and excellent ductility (10% fracture strain at 350 ℃) with negligible LME susceptibility, the fracture surface features uniform dimples, indicative of ductile fracture. In contrast, at 550 ℃, mechanical performance deteriorates drastically (fracture strength: 410 MPa, fracture strain: 5%) with typical LME-induced damage, and the flat fracture surface exhibits cleavage/intergranular brittle fracture characteristics.

(2). The corrosion mechanism is temperature-controlled: At 350 ℃ and 450 ℃, a protective oxide layer composed of Al and Cr is formed, which can hinder the penetration of LBE; however, when the temperature rises to 550 ℃, the oxide layer is damaged, Cr and Al elements dissolve, and enrichment of Pb and Bi elements occurs at the interface. This exacerbates LBE corrosion, thereby triggering LME.

(3). Good matrix stability: No obvious segregation or massive loss of Al, Cr, Fe, Co, and Ni is observed, and the alloy matrix does not undergo severe compositional degradation. At different temperatures, its corrosion resistance is superior to that of traditional austenitic stainless steels and ferritic/martensitic steels.

(4). Potential Industrial Applications: The $Al_{0.1}$CoCrFeNi HEA exhibits favorable corrosion resistance, chemical stability, and resistance to LME in liquid LBE environments. Therefore, it shows potential as a candidate material for LFRs, accelerator-driven systems (ADSs), and liquid-metal heat exchange equipment, providing a material basis and design reference for key components and surface/interface protection in next-generation nuclear energy systems.

Author Contributions

S.X.: Conceptualization, Methodology, Investigation, Supervision, Funding Acquisition, Writing-Review & Editing. Y.Y.: Investigation, Data Curation Writing-Review & Editing. B.W.: Writing-Review & Editing. X.Z.: Writing-Review & Editing.

Funding

The work is financially supported by the Key R&D and Transformation Plan of Qinghai Province (2025-QY-241), the Fundamental Research Funds for the Central Universities (2024MS049), and State Key Laboratory of Nuclear Physics and Technology, Peking University (NPT2023KFY09).

Institutional Review Board Statement

Not applicable.

Informed Consent Statement

Not applicable.

Data Availability Statement

The data supporting the findings of this study are available from the corresponding author upon reasonable request.

Conflicts of Interest

The authors declare no conflict of interest.

Use of AI and AI-Assisted Technologies

No AI tools were utilized for this paper.

References

1. Abram, T.; Ion, S. Generation-IV nuclear power: A review of the state of the science. *Energy Policy* **2008**, *36*, 4323–4330. https://doi.org/10.1016/j.enpol.2008.09.059.
2. Concetta, F. Introduction. In *Handbook on Lead-bismuth Eutectic Alloy and Lead Properties, Materials Compatibility, Thermal-hydraulics and Technologies: 2015 Edition*; Nuclear Energy Agency: Moulineaux, France, 2015. https://doi.org/org/10.1787/42dcd531-en.
3. Lorusso, P.; Bassini, S.; Del Nevo, A.; et al. GEN-IV LFR development: Status & perspectives. *Prog. Nucl. Energy* **2018**, *105*, 318–331. https://doi.org/10.1016/j.pnucene.2018.02.005.
4. Wang, W.; Yang, C.; You, Y.; Yin, H. A Review of Corrosion Behavior of Structural Steel in Liquid Lead–Bismuth Eutectic. *Crystals* **2023**, *13*, 968. https://doi.org/10.3390/cryst13060968.
5. Gong, X.; Li, R.; Sun, M.; et al. Opportunities for the LWR ATF materials development program to contribute to the LBE-cooled ADS materials qualification program. *J. Nucl. Mater.* **2016**, *482*, 218–228. https://doi.org/10.1016/j.jnucmat.2016.10.012.
6. Tsisar, V.; Schroer, C.; Wedemeyer, O.; et al. Long-term corrosion of austenitic steels in flowing LBE at 400 °C and 10^{-7} mass% dissolved oxygen in comparison with 450 and 550 °C. *J. Nucl. Mater.* **2016**, *468*, 305–312. https://doi.org/10.1016/j.jnucmat.2015.09.027.
7. Lambrinou, K.; Charalampopoulou, E.; Van der Donck, T.; et al. Dissolution corrosion of 316L austenitic stainless steels in contact with static liquid lead-bismuth eutectic (LBE) at 500 °C. *J. Nucl. Mater.* **2017**, *490*, 9–27. https://doi.org/10.1016/j.jnucmat.2017.04.004.
8. Lambrinou, K.; Koch, V.; Coen, G.; et al. Corrosion scales on various steels after exposure to liquid lead-bismuth eutectic. *J. Nucl. Mater.* **2013**, *450*, 244–255. https://doi.org/10.1016/j.jnucmat.2013.09.034.
9. Hosemann, P.; Frazer, D.; Stergar, E.; et al. Twin boundary-accelerated ferritization of austenitic stainless steels in liquid lead–bismuth eutectic. *Scr. Mater.* **2016**, *118*, 37–40. https://doi.org/10.1016/j.scriptamat.2016.02.029.
10. Tsisar, V.; Gavrilov, S.; Schroer, C.; et al. Long-term corrosion performance of T91 ferritic/martensitic steel at 400 °C in flowing Pb-Bi eutectic with 2×10^{-7}mass% dissolved oxygen. *Corros. Sci.* **2020**, *174*, 108852. https://doi.org/10.1016/j.corsci.2020.108852.
11. Balbaud, F.; Martinelli, L. Corrosion issues in lead-cooled fast reactor (LFR) and accelerator driven systems (ADS). In *Nuclear Corrosion Science and Engineering*; Woodhead Publishing Limited: Sawston, UK, 2012; pp. 807–841. https://doi.org/10.1533/9780857095343.6.807.
12. Martinelli, L.; Balbaud-Célérier, F.; Terlain, A.; et al. Oxidation mechanism of a Fe-9Cr-1Mo steel by liquid Pb-Bi eutectic alloy (Part I). *Corros. Sci.* **2008**, *50*, 2523–2536. https://doi.org/10.1016/j.corsci.2008.06.050.
13. Hojná, A.; Halodová, P.; Chocholoušek, M.; et al. Environmentally assisted cracking of T91 ferritic-martensitic steel in heavy liquid metals. *Corros. Rev.* **2020**, *38*, 183–194. https://doi.org/10.1515/corrrev-2019-0035.
14. Gong, X.; Marmy, P.; Verlinden, B.; et al. Low cycle fatigue behavior of a modified 9Cr-1Mo ferritic-martensitic steel in lead–bismuth eutectic at 350 °C—Effects of oxygen concentration in the liquid metal and strain rate. *Corros. Sci.* **2015**, *94*, 377–391. https://doi.org/10.1016/j.corsci.2015.02.022.
15. Gong, X.; Chen, J.; Xiang, C.; et al. A comparative study on liquid metal embrittlement susceptibility of three FeCrAl ferritic alloys in contact with liquid lead-bismuth eutectic at 350 °C. *Corros. Sci.* **2021**, *183*, 109346. https://doi.org/10.1016/j.corsci.2021.109346.
16. Gong, X.; Chen, J.; Hu, F.; et al. Liquid metal embrittlement of an Fe10Cr4Al ferritic alloy exposed to oxygen-depleted and -saturated lead-bismuth eutectic at 350 °C. *Corros. Sci.* **2020**, *165*, 108364. https://doi.org/10.1016/j.corsci.2019.108364.
17. Zhang, J.; Li, N. Review of the studies on fundamental issues in LBE corrosion. *J. Nucl. Mater.* **2008**, *373*, 351–377. https://doi.org/10.1016/j.jnucmat.2007.06.019.
18. Yao, C.; Wang, Z.; Zhang, H.; et al. HLMIF, a facility for investigating the synergistic effect of ion-irradiation and LBE corrosion. *J. Nucl. Mater.* **2019**, *523*, 260–267. https://doi.org/10.1016/j.jnucmat.2019.05.049.

19. Stergar, E.; Eremin, S.G.; Gavrilov, S.; et al. Influence of LBE long term exposure and simultaneous fast neutron irradiation on the mechanical properties of T91 and 316L. *J. Nucl. Mater.* **2016**, *473*, 28–34. https://doi.org/10.1016/j.jnucmat.2016.02.008.
20. Yeh, J.W.; Chen, S.K.; Lin, S.J.; et al. Nanostructured High-Entropy Alloys with Multiple Principal Elements: Novel Alloy Design Concepts and Outcomes. *Adv. Eng. Mater.* **2004**, *6*, 299–303. https://doi.org/10.1002/adem.200300567.
21. George, E.P.; Curtin, W.A.; Tasan, C.C. High entropy alloys: A focused review of mechanical properties and deformation mechanisms. *Acta Mater.* **2020**, *188*, 435–474. https://doi.org/10.1016/j.actamat.2019.12.015.
22. Li, Z.; Zhao, S.; Ritchie, R.O.; et al. Mechanical properties of high-entropy alloys with emphasis on face-centered cubic alloys. *Prog. Mater. Sci.* **2019**, *102*, 296–345. https://doi.org/10.1016/j.pmatsci.2018.12.003.
23. Sathiyamoorthi, P.; Kim, H.S. High-entropy alloys with heterogeneous microstructure: Processing and mechanical properties. *Prog. Mater. Sci.* **2020**, *123*, 100709. https://doi.org/10.1016/j.pmatsci.2020.100709.
24. Shi, Y.; Collins, L.; Feng, R.; et al. Homogenization of $Al_xCoCrFeNi$ high-entropy alloys with improved corrosion resistance. *Corros. Sci.* **2018**, *133*, 120–131. https://doi.org/10.1016/j.corsci.2018.01.030.
25. Luo, H.; Lu, W.; Fang, X.; et al. Beating hydrogen with its own weapon: Nano-twin gradients enhance embrittlement resistance of a high-entropy alloy. *Mater. Today* **2018**, *21*, 1003–1009. https://doi.org/10.1016/j.mattod.2018.07.015.
26. Zhao, Y.; Lee, D.-H.; Seok, M.-Y.; et al. Resistance of CoCrFeMnNi high-entropy alloy to gaseous hydrogen embrittlement. *Scr. Mater.* **2017**, *135*, 54–58. https://doi. org/ 10.1016/j.scriptamat.2017.03.029.
27. Jin, K.; Lu, C.; Wang, L.M.; et al. Effects of compositional complexity on the ion-irradiation induced swelling and hardening in Ni-containing equiatomic alloys. *Scr. Mater.* **2016**, *119*, 65–70. https://doi.org/10.1016/j.scriptamat.2016.03.030.
28. Yang, T.; Guo, W.; Poplawsky, J.D.; et al. Structural damage and phase stability of Al0.3CoCrFeNi high entropy alloy under high temperature ion irradiation. *Acta Mater.* **2020**, *188*, 1–15. https://doi.org/10.1016/j.actamat.2020.01.060.
29. Yang, T.; Xia, S.; Liu, S.; et al. Effects of AL addition on microstructure and mechanical properties of $Al_xCoCrFeNi$ High-entropy alloy. *Mater. Sci. Eng. A* **2015**, *648*, 15–22. https://doi.org/10.1016/j.msea.2015.09.034.
30. Rao, J.C.; Diao, H.Y.; Ocelík, V.; et al. Secondary phases in $Al_xCoCrFeNi$ high-entropy alloys: An in-situ TEM heating study and thermodynamic appraisal. *Acta Mater.* **2017**, *131*, 206–220. https://doi.org/10.1016/j.actamat.2017.03.066.
31. Lu, J.; Chen, Y.; Zhang, H.; et al. Effect of Al content on the oxidation behavior of Y/Hf-doped AlCoCrFeNi high-entropy alloy. *Corros. Sci.* **2020**, *170*, 108691. https://doi.org/10.1016/j.corsci.2020.108691.
32. Xing, G.; Haitao, C.; Feifei, Z.; et al. Degradation of tensile mechanical properties of two AlxCoCrFeNi (x = 0.3 and 0.4) high-entropy alloys exposed to liquid lead-bismuth eutectic at 350 and 500 °C. *J. Nucl. Mater.* **2021**, *558*, 153364. https://doi.org/10.1016/j.jnucmat.2021.153364.
33. Gorse, D.; Auger, T.; Vogt, J.B.; et al. Influence of liquid lead and lead–bismuth eutectic on tensile, fatigue and creep properties of ferritic/martensitic and austenitic steels for transmutation systems. *J. Nucl. Mater.* **2011**, *415*, 284–292. https://doi.org/10.1016/j.jnucmat.2011.04.047.
34. Gao, Z.; Xue, L.; Peng, X.; et al. Enhanced compatibility of Al-modulated $Al_xNiCoFeCr$ high-entropy alloy and microstructure degradation under static oxygen-saturated lead bismuth eutectic. *J. Alloys Compd.* **2025**, *1037*, 182253. https://doi.org/ 10.1016/j.jallcom.2025.182253.
35. Shahboub, A.; Chen, P.; Deng, C.; et al. Investigation of the anti-corrosion behavior of Fe-Cr oxide layer in LBE: A first-principles study. *J. Nucl. Mater.* **2025**, *605*, 155592. https://doi.org/10.1016/j.jnucmat.2024.155592.
36. Gong, X.; Short, M.P.; Auger, T.; et al. Environmental degradation of structural materials in liquid lead- and lead-bismuth-eutectic-cooled reactors. *Prog. Mater. Sci.* **2022**, *126*, 100920. https://doi.org/10.1016/j.pmatsci.2022.100920.